

The ASTRA project: a doorway to future astrometry

M. Gai^a, Z. Qi^b, M.G. Lattanzi^a, B. Bucciarelli^a, D. Busonero^a, M. Crosta^a, F. Landini^a, S. Liao^b, H. Luo^b, G. Mana^c, R.A. Méndez^d, M. Pisani^c, A. Riva^a, C. San Martin Luque^d, C.P. Sasso^c, Z. Tang^b, A. Vecchiato^a, Y. Yu^b

^aINAF - Osserv. Astrofisico di Torino, V. Osservatorio, 20, I-10025 Pino Torinese (TO), Italy

^bShanghai Astronomical Observatory, CAS, 80 Nandan Rd, Shanghai 200030, China

^cINRiM - Ist. Naz. di Ricerca Metrologica, Str. delle Cacce, 91, I-10135 Torino (TO), Italy

^dDepartamento de Astronomia, Universidad de Chile, Casilla 36-D, Santiago, Chile

ABSTRACT

Astrometric Science and Technology Roadmap for Astrophysics (ASTRA) is a bilateral cooperation between China and Italy with the goal of consolidating astrometric measurement concepts and technologies. In particular, the objectives include critical analysis of the Gaia methodology and performance, as well as principle demonstration experiments aimed at future innovative astrometric applications requiring high precision over large angular separations (one to 180 degrees). Such measurement technologies will be the building blocks for future instrumentation focused on the “great questions” of modern cosmology, like General Relativity validity (including Dark Matter and Dark Energy behavior), formation and evolution of structure like proto-galaxies, and planetary systems formation in bio compatibles environments. We describe three principle demonstration tests designed to address some of the potential showstoppers for high astrometric precision experiments. The three tests are focused on the key concepts of multiple fields telescopes, astrometric metrology and very fine sub-pixel precision (goal: $< 1/2000$ pixel) in white light.

Keywords: ASTRA, Fundamental Physics, Metrology

1. INTRODUCTION

This paper describes the scope and the initial activity of the ASTRA (Astrometric Science and Technology Roadmap for Astrophysics) project. ASTRA is a collaboration between the Italian Institute for Astrophysics (INAF), in particular the astrometric team at the Astrophysical Observatory of Turin (OATo), and the Shanghai Astronomical Observatory (SHAO, Chinese Academy of Sciences - CAS), under the auspices of their respective Ministries, in the framework of the Scientific and Technological Cooperation Agreement between China and Italy. The project, started in late 2019, builds on a long collaboration between the teams in the field of high precision astrometry, in particular on materialization of the absolute reference frame (APOP,¹), the astrometry mission proposal GAME (Gravitation Astrometric Measurement Experiment) to ESA,^{2,3,4} its 2015 AGP (Astrometric Gravitation Probe) rendition,⁵ and the ongoing experience on Gaia.^{6,7,8} ASTRA also aims at fostering and consolidating national and international collaborations on astronomical and interdisciplinary research related to astrometric advancement.

The “great questions” of modern Cosmology, summarising e.g. ESA’s Cosmic Vision “Grand Themes”, are:

1. Validity of General Relativity (GR) at all scales, hence the nature of Dark Matter and Dark Energy and their relationship with baryonic structures;
2. structure formation and evolution, from primordial galaxies to the Milky Way; study of distant and local gravitational wave sources;
3. formation of planetary systems (including the Solar System) and life supporting environments.

Further author information: E-mail: mario.gai@inaf.it, Telephone: +39 011 8101 943, www.oato.inaf.it; E-mail: zxqi@shao.ac.cn, Telephone: +86 21 3477 5203, english.shao.cas.cn

The main goal of ASTRA is the deployment of shared experience on enabling astrometric technologies aimed at future large angle, high precision measurements. The activity is based on synergy of science and technology: we will build on our GR models for the Gaia mission, to consolidate science requirements for astrometric technology:^{9,10} measurement at $< 1 \mu\text{as}$ implies simulation accuracy in the range 0.1 to $0.1 \mu\text{as}$ to ensure control of model errors. The long-term objective is the development of innovative astronomic instrumentation reliably operating in the micro-arcsecond (μas) precision range or better, also including relativistic experiments, as the above mentioned GAME/AGP, or a novel astrometric instrument concept presented in another contribution to this meeting (RAFTER,¹¹). This will be achieved through modelization, simulation and laboratory experiments, addressing some basic implementation aspects of astrometric measurements, described below.

The ASTRA activity follows an historical path started with Hipparcos,¹² continues with Gaia, and aims toward future groundbreaking experiments on astrophysics and fundamental physics, e.g. JWST,¹³ NEAT,¹⁴ Theia,¹⁵ Gaia extensions to higher precision or other spectral bands, in particular NIR,¹⁶ and others.^{11,17} The main output of ASTRA will be a white paper summarising a roadmap toward future high precision astrometry.

Modern astrophysical instrumentation aims at photon limit precision. Current missions (like Gaia and Euclid) probably exploit present technological limits on passive stabilization, while future ones (like LISA), based on distributed instruments, intrinsically rely on advanced metrology concepts. Observing fairly bright stars ($V = 8 - 10 \text{ mag}$) in the visible range, a 1 m class telescope can achieve a nominal μas level precision in a fairly short exposure time, of order of one hour. In practice, comparable accuracy, i.e. systematic error control, is hard to achieve. This is related to knowledge of the instrument response throughout the measurement, hence calibration. Moderate variation of the instrument response over the field of view, observing bandwidth, and in time, are of course beneficial toward good modeling and reliable estimation of instrumental parameters, therefore usually stringent requirements are issued on imaging quality and stability.

Among the main challenges considered for (sub-) μas astrometry, relevant sources of systematic errors are:

1. the field variation of telescope optical response;
2. the variation of electro-optical response over detectors;
3. “Cosmic noise”, i.e. the (real or apparent) variability of individual astronomical objects.

Moreover, the capability of large angle measurement (a few to several ten degrees) is a crucial requirement either in the context of global astrometry (with the approach of Hipparcos and Gaia), or looking for adequate, typically bright, reference sources.

The ASTRA study includes a critical review of reference science goals, deriving a detailed definition of scientific requirements, also taking advantage of the lessons learned from Gaia, and setting the specifications for relevant aspects of future applications.

As a possible mitigation strategy with respect to the above challenges, we investigate the concept of an annular field telescope, RAFTER: Ring Astrometric Field Telescope for Exo-planets and Relativity.¹¹ It features highly uniform optical response over a large focal plane area, thus providing favourable characteristics with respect to the possibility of averaging out detector and source variability over a set of observations. A specific application for Fundamental Physics, with the addition of a custom coronagraphic system, is represented by the current Astrometric Gravitation Probe design.¹⁸

1.1 Technological objectives

The above critical aspects have been assessed^{19,20} in the literature; in the context of ASTRA, three specific concepts will be tested as potential contributions toward systematics control. They are described in the following sections, and can be summarized as:

1. multiple line-of-sight (LOS) telescopes: study, optimization and prototyping of a three LOS telescope, compatible with metrology, to materialize the bidimensional angular gauge onto the sky;

2. astrometric metrology: a high precision metrology device strictly embedded in the telescope design, for the real-time estimation²¹ of systematic error induced by external sources, using BAM-like²² fringes;
3. image centering experiment: design, simulation, implementation and data analysis of a setup for high precision location of images on CCD and CMOS detectors, down to $1 < 2000$ pixel, through calibration and differential techniques.

2. EXPERIMENT DESCRIPTION

The first period of activity is mostly focused on implementation of the Image Centering Experiment described in Sec. 2.1, whereas the other aspects are investigated at the moment mostly at the level of design and simulation.

2.1 Image Centering Experiment

The principle is similar to that implemented in Gai et al. (2001),²³ and consists in the simplest representation of an imaging instrument, i.e. a camera fed by a doublet, observing a simulated stellar field. The setup also has some educational value, e.g. allowing students to get hands-on experience on the problem without consuming precious telescope time.

The expected result on location uncertainty are described in the literature,^{23,24,25} and its relationship with the theoretical Cramér-Rao limit is also discussed in other papers.^{26,27} In practice, the image photocenter, in low background conditions, is affected by errors depending on geometric factors related to the PSF shape, and scaling inversely to the SNR, at least for bright sources. For a Gaussian PSF²⁴ centered in x_c , with Gaussian width σ :

$$\Phi(x; x_c, \sigma) = \frac{1}{\sqrt{2\pi}\sigma} \exp \left[-\frac{(x - x_c)^2}{2\sigma^2} \right]. \quad (1)$$

the location uncertainty σ_c is

$$\sigma_c \geq \frac{\sigma}{SNR}. \quad (2)$$

Similar expressions can be achieved for large classes of PSF shapes, replacing the Gaussian width σ with a geometric factor, expressed e.g. as a function of the diffraction parameter λ/D , to be computed^{28,29} according to imaging performance and measurement conditions. Although Eq. 2 is rather general, the dependence on source magnitude, readout noise, background and actual PSF shape is totally implicit; more detail can be found in the above literature and references therein.

In the framework of our collaboration, two versions of the same concept have been realized, in each Institute's labs. They are similar but not identical, in order to cover a wider range of possible choices. Measurements will be taken with both CMOS and CCD sensors, in order to evidence some of the characteristics of each technology. In both versions, since the source images are significantly smaller than the detector area, it is possible to perform response tests over large fractions of the detector sensitive area simply by offsetting the camera, i.e. implementing a sort of dithering strategy in the lab. The simulated stellar field takes therefore the role of conventional test patterns in commercial imaging applications. The SHAO version also features comparable brightness of all artificial stars, whereas the OATo version generates sources on a range of about three magnitudes.

2.1.1 SHAO implementation

The SHAO version adopts an array of fibers arranged in a regular grid, reimaged onto a Sony QHY4040 CMOS camera (front illuminated sensor, $4k \times 4k$ format, pixel size $9 \mu m$), according to the scheme depicted in Fig. 1. The resulting images occupy a limited detector region (about 350×350 pixels), and two sample frames are shown in Fig. 2 (log scale). The spots are oversampled, in order to reduce the sensitivity to pixel response variation; this also provides a larger dynamic range. The image quality variation over the field is negligible.

The pupil size is set to approximately 2 mm, and the light source, very bright, required neutral filters required to prevent saturation even with the shortest exposure time [1 ms] made available by the camera control electronics. Alignment and focusing are undergoing optimization.

The image quality is dominated by the resolved fiber core, providing a Gaussian spot with size $\sigma \simeq 6$ pixel. The

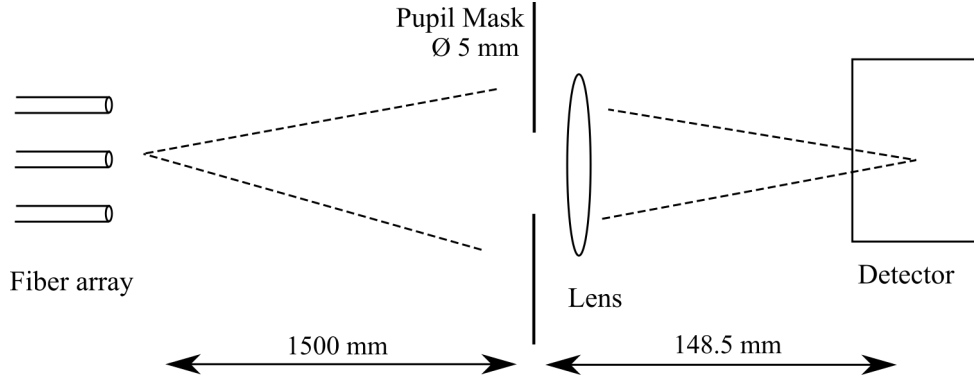


Figure 1. Optical layout of SHAO image centering experiment (not to scale).

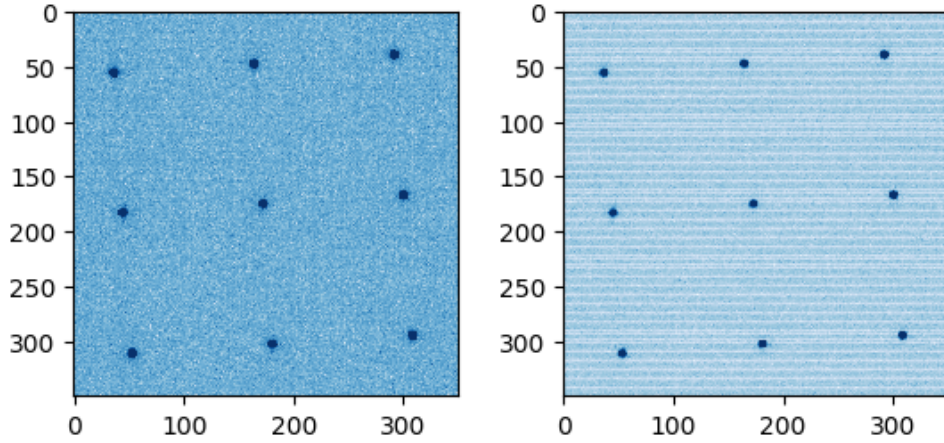


Figure 2. Field image of SH location experiment, log scale; normal frame (left), and frame affected by excess spatial noise (right).

fiber array is not aligned with the detector axes. In the preliminary integration and alignment test, four short sequences of full frames were taken, at the maximum rate of 10 frames/s.

The preliminary evaluation of the images evidenced a comparably large spatial noise (~ 90 ADU), not justified by the background level (~ 1700 ADU) and nominal readout noise (~ 4 electrons). The trouble is likely due to environmental EM noise, whose source is under investigation. In spite of such significant noise, the image location is reasonably good.

The location algorithms used to process the image set are a simple center-of-gravity (COG), and gaussian fit. They provide quite similar results, as expected from the Gaussian image shape and high SNR conditions, but the latter provides of course somewhat lower sensitivity to the spatial noise excess experienced on some frames. Dispersion, shown in Fig. 3, is mainly due to common mode drift of order of 0.1 pixel, mostly over the X axis. Removal of the common mode significantly abates the dispersion, to the order of 0.01 pixel, somewhat larger on the Y axis. The residual photo-center dispersion is shown as a scatter plot in Fig. 4, and as a set of stacked histogram in Fig. 5. All simulated star, with approximately the same brightness and signal level, have comparable dispersion.

The statistics on photo-center dispersion is reported in Table 1, in which the standard deviation of initial source positions in frame coordinates is reported as X(Y) Raw. The RMS coordinate residual after common mode subtraction, corresponding to fluctuation with respect to the overall motion of the set of stars, is reported as

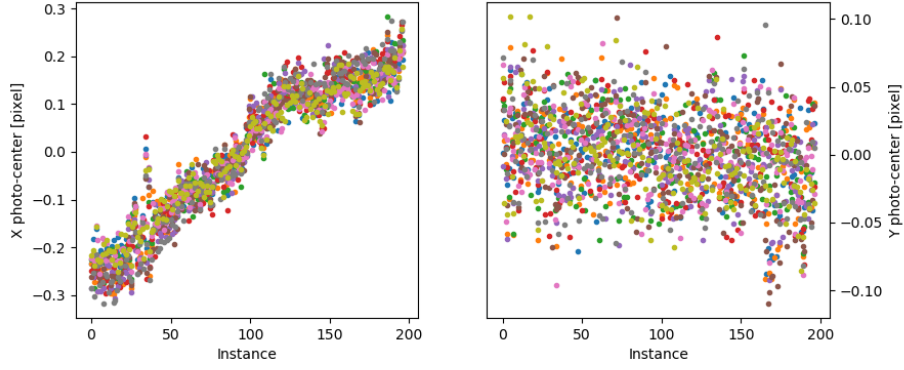


Figure 3. Raw photo-center dispersion, along X (left) and Y (right) [SH].

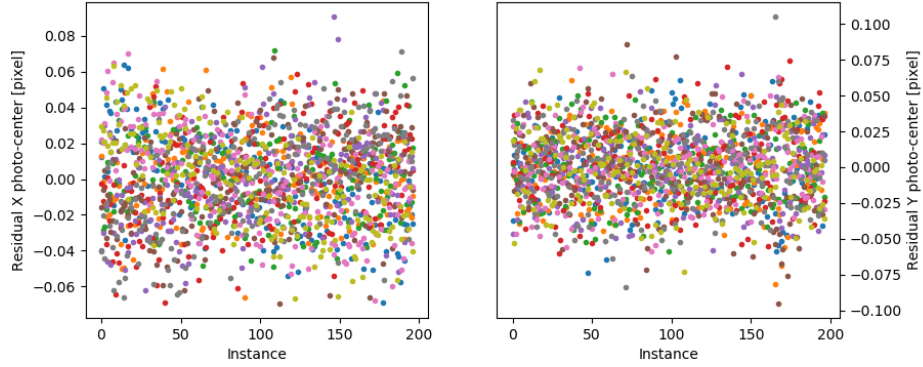


Figure 4. Residual photo-center dispersion, along X (left) and Y (right), after common mode removal [SH].

X(Y) Res, and can be compared with the corresponding Cramér-Rao limiting value X(Y) CRL in the subsequent line; the ratio between the two values is reported as X(Y) Rel.

Table 1. Location performance statistics on X and Y photo-center. Raw: uncorrected estimates; Res.: common mode subtracted; CRL: Cramér-Rao limit; Rel.: ratio between measured dispersion and Cramér-Rao limit [SH].

| | 1 | 2 | 3 | 4 | 5 | 6 | 7 | 8 | 9 |
|------------|--------|--------|--------|--------|--------|--------|--------|--------|--------|
| X Raw [px] | 0.1332 | 0.1495 | 0.1470 | 0.1579 | 0.1590 | 0.1541 | 0.1311 | 0.1634 | 0.1308 |
| Y Raw [px] | 0.0295 | 0.0316 | 0.0287 | 0.0309 | 0.0295 | 0.0375 | 0.0286 | 0.0303 | 0.0314 |
| X Res [px] | 0.0256 | 0.0225 | 0.0216 | 0.0268 | 0.0262 | 0.0253 | 0.0264 | 0.0285 | 0.0267 |
| X CRL [px] | 0.0191 | 0.0196 | 0.0207 | 0.0211 | 0.0217 | 0.0215 | 0.0197 | 0.0202 | 0.0226 |
| X Rel | 1.3443 | 1.1450 | 1.0453 | 1.2724 | 1.2040 | 1.1754 | 1.3410 | 1.4109 | 1.1807 |
| Y Res [px] | 0.0245 | 0.0246 | 0.0226 | 0.0272 | 0.0232 | 0.0289 | 0.0229 | 0.0273 | 0.0251 |
| Y CRL [px] | 0.0189 | 0.0213 | 0.0210 | 0.0206 | 0.0227 | 0.0218 | 0.0196 | 0.0204 | 0.0225 |
| Y Rel | 1.2973 | 1.1520 | 1.0756 | 1.3220 | 1.0207 | 1.3280 | 1.1671 | 1.3372 | 1.1171 |

The experimental dispersion X(Y) Res ranges between a few percent and a few ten percent above the theoretical best performance X(Y) CRL; the variation appears to be due to (a) actual image shape not exactly Gaussian, (b) approximate SNR estimation, and (c) unmodelled effects of spatial noise.

The results match the expectations for the observation SNR (~ 300) and Gaussian image profile shape ($\sigma \simeq 6$ pixels), within the simple assumptions applied. The location dispersion, of order of $1/50$ pixel, correspond to

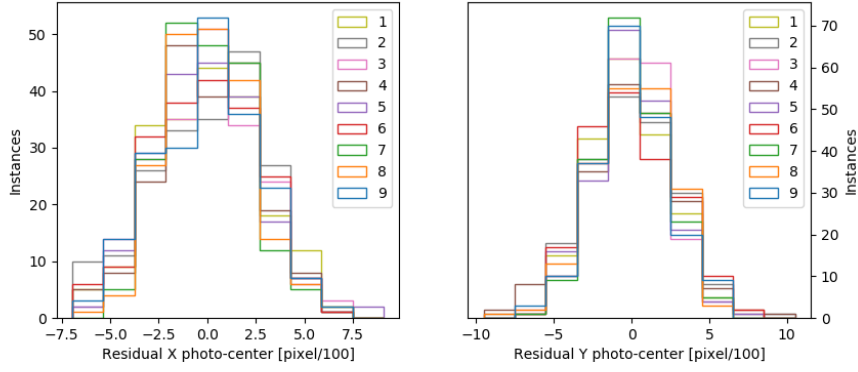


Figure 5. Residual photo-center histogram, along X (left) and Y (right), after common mode removal [SH].

about 1/500 of the actual image width, due to the oversampling.

2.1.2 OATo implementation

The OATo version uses a lab LED source (Thorlabs M625L4, nominal wavelength 625 nm, bandwidth 17 nm) and a custom array of pinholes irregularly spaced, reimaged onto a Kiralux CS235MU CMOS Camera ($1,920 \times 1,200$ format, pixel size $5.86 \mu\text{m}$), according to the scheme depicted in Fig. 6. The pinhole array is the same used in activity for a previous publication.³⁰ The resulting images occupy a limited detector region (about 800×850 pixels), and a sample frame is shown in Fig. 7 (left); the right panel shows a zoomed version of the nine spots. The images are nearly diffraction limited, since up to four diffraction rings are clearly visible, on the brightest sources, around the central peak. The image quality variation over the field is negligible.

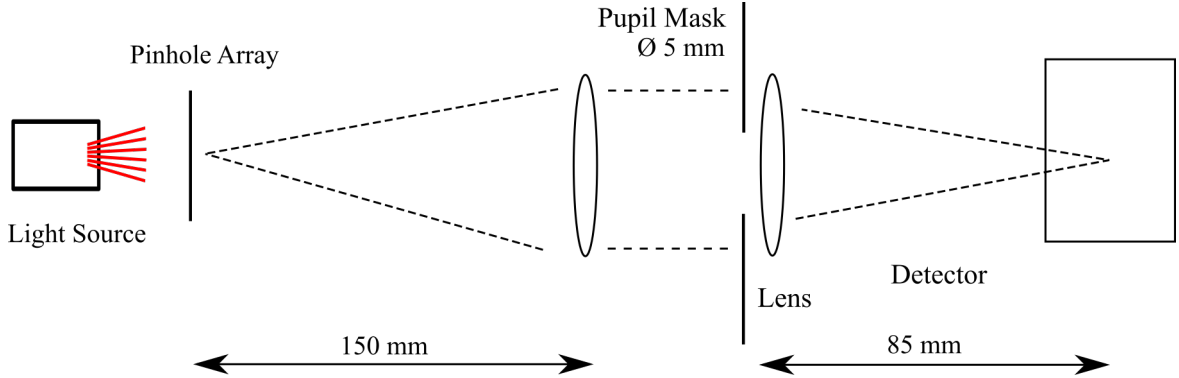


Figure 6. Optical layout of OATo location experiment (not to scale).

The pupil size is again $\sim 2 \text{ mm}$, and the source is sufficiently bright to ensure a signal level reaching a reasonable fraction of the full dynamic range with 10 ms exposures; due to the different illumination of the pinholes, the photon flux of the simulated sources ranges over about one order of magnitude.

The background level, after partial optimization, is $\sim 2 \text{ ADU}$, with much lower spatial noise (a few ADU) than experienced in the previous setup, thus comparing well with the nominal RON ($\sim 1 \text{ ADU}$). The analysis below refers to a set of 100 frames collected in stable environment conditions.

The location algorithms (apart COG for preliminary tests) are unweighted least square (LSQ) and maximum likelihood (ML) fit to the nominal polychromatic PSF of an ideal circular aperture, estimating PSF radius, photo-centre position and background. In the ML framework, we also estimate the expected error (MLEE), using expressions consistent with those derived e.g. in the 1D case in Gai et al., 2017.²⁵

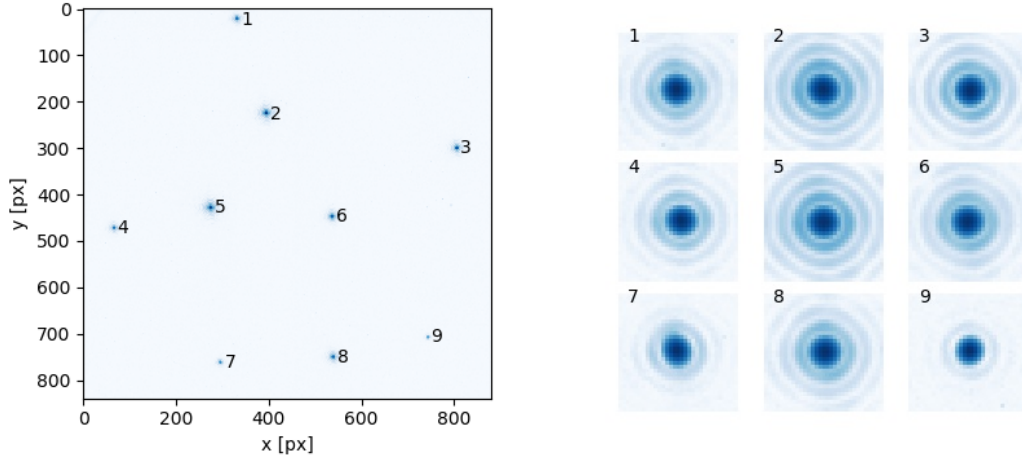


Figure 7. Field image (log scale) of (left), and zoomed view of the nine spots (right).

Since the camera dynamic range is limited to 12 bits, it was not possible to increase significantly the analogic integration; we therefore explore the option of digital integration by stacking the frames four at a time, mimicking the results of a fourfold increase in the exposure time. In the best case of purely random noise, with low systematics, this should improve the measurement precision by a factor two. The processing results from individual and stacked frames are labelled by “I” and “S”, respectively.

Table 2. Location performance statistics on X and Y photo-center, using the Maximum Likelihood estimator on individual frames (I) and on 4-by-4 stacked images (S) [TO]. Raw: uncorrected estimates; Res.: common mode subtracted; MLEE: Maximum Likelihood Expected Error. Units: 1/100 pixel.

| | 1 | 2 | 3 | 4 | 5 | 6 | 7 | 8 | 9 |
|---------|-------|-------|-------|-------|-------|-------|-------|-------|-------|
| X I Raw | 2.093 | 1.908 | 2.195 | 1.736 | 1.783 | 2.022 | 2.014 | 1.969 | 2.387 |
| Y I Raw | 2.523 | 2.393 | 2.582 | 2.055 | 2.275 | 2.410 | 2.436 | 2.193 | 2.744 |
| X I Res | 0.853 | 0.507 | 1.072 | 1.005 | 0.531 | 0.563 | 1.113 | 0.657 | 1.684 |
| X MLEE | 0.644 | 0.284 | 0.327 | 0.415 | 0.278 | 0.494 | 1.144 | 0.503 | 1.673 |
| Y I Res | 0.986 | 0.617 | 0.706 | 0.814 | 0.478 | 0.494 | 1.513 | 0.873 | 1.954 |
| Y MLEE | 0.642 | 0.294 | 0.322 | 0.444 | 0.289 | 0.509 | 1.032 | 0.499 | 1.545 |
| X S Raw | 1.071 | 1.058 | 1.333 | 0.823 | 0.958 | 1.057 | 0.939 | 1.089 | 1.355 |
| Y S Raw | 2.083 | 1.984 | 2.045 | 1.705 | 1.887 | 1.951 | 1.600 | 1.702 | 1.626 |
| X S Res | 0.336 | 0.266 | 0.734 | 0.479 | 0.374 | 0.183 | 0.591 | 0.290 | 0.846 |
| Y S Res | 0.489 | 0.274 | 0.344 | 0.396 | 0.274 | 0.294 | 0.617 | 0.466 | 0.994 |

As in the case of the SHAO implementation, the standard deviation of raw photo-centre estimates, listed in Table 2 and labelled “Raw”, appears to be dominated by a significant common mode motion, somewhat reduced with minor improvements on mounting mechanics to the order of 0.02 pixel. After common mode subtraction, the dispersion of residuals (“Res”) is reduced by a significant factor, below the 0.01 pixel level.

A representation of the different level of location error is shown in Fig. 8, where residual photo-centre values are shown as displacement with respect to the nominal frame positions (not to scale), respectively for individual (left) and stacked (right) images. The apparent size of the cloud of points is significantly reduced in the latter case.

Image stacking actually provides an improvement on photo-centre dispersion by a factor close to the expected value two, although the difference among sources is large. Also, the dispersion of residuals from individual frames compares well with the predicted MLEE, although the difference between theory and experiment is quite different

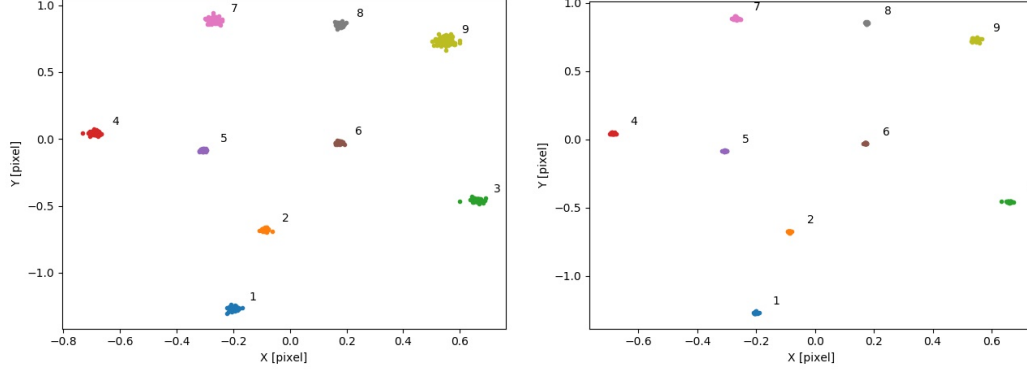


Figure 8. Scatter plot of star location dispersion around the nominal position (not to scale) for individual (left) and stacked (right) frames [TO].

for different sources, ranging from few percent to a factor two. In some cases, the experimental spread is even slightly lower than the MLEE. This appears to be related to the unmodelled sources of error, e.g. the crude image model, field dependent perturbations, and the limited statistics.

The location uncertainty is shown in Fig. 9 as a function of the instrumental magnitude, including the results from both individual and stacked frames. The overall trend is roughly in agreement with the nominal behaviour suggested by theory, i.e. a linear dependence.

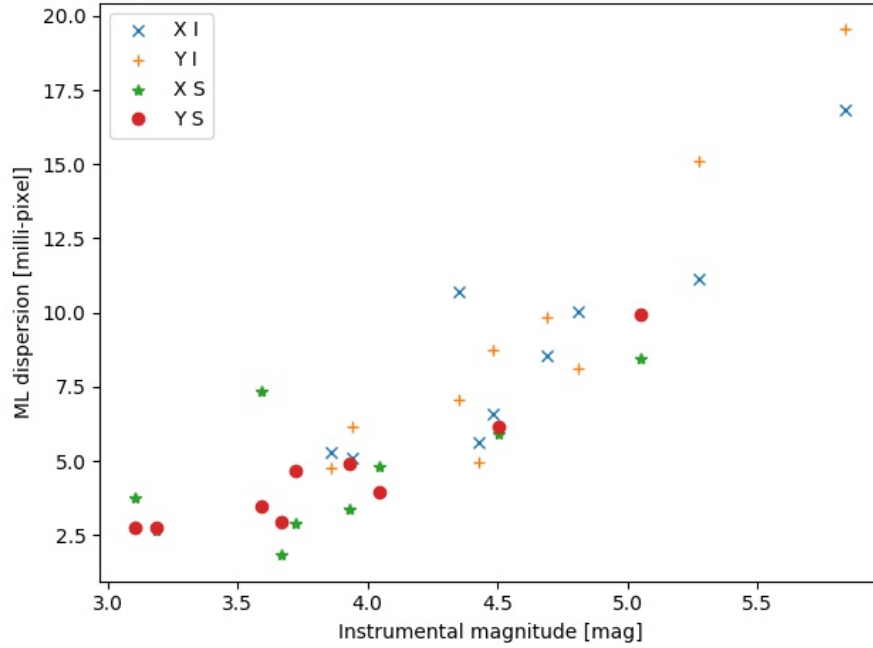


Figure 9. Location dispersion of individual and stacked images vs. instrumental magnitude [TO].

2.2 Metrology Embedded in Telescope

Metrology is being used in the Gaia Basic Angle Monitoring (BAM) device²² to keep track of instrument perturbations, small with respect to the scale of conventional imaging quality, but relevant to the astrometric error budget. The BAM noise performance was specified at the level of a few μas over the timescale of a few minutes.

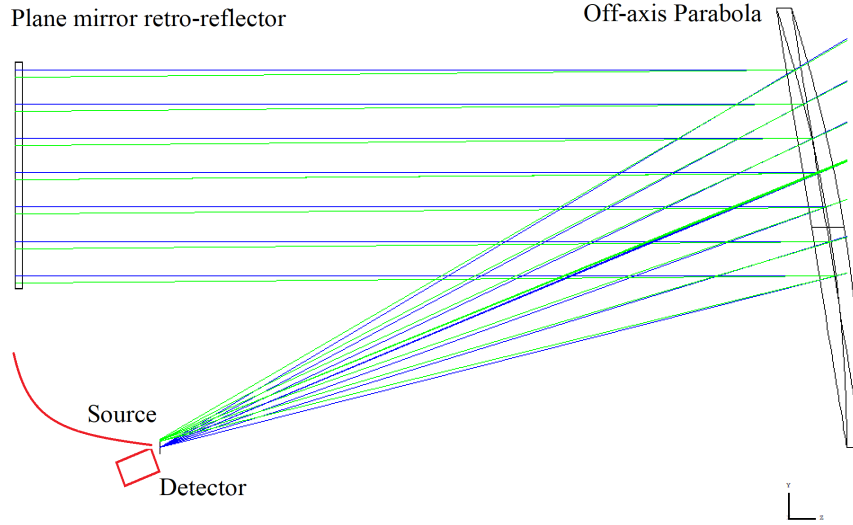


Figure 10. Schematic of auto-collimation metrology experiment.

In the case of Gaia, the conceptual requirement is to measure the angle (or its variation) between the LOS of two telescopes.

In principle, the LOS is affected by perturbations of any parameter of the optical system, although by different amounts which can be estimated by sensitivity analysis. A beam combiner removes, at first order, the basic angle issue from the telescope and embeds it into a separate subsystem, which might have simple geometry and thus hopefully ensure adequate stability thanks to robust mechanical implementation.

The passive stability approach was sufficient for Hipparcos, designed with a precision goal in the $0.1 \text{ milli-arcsec (mas)}$ range, but it was no longer adequate for Gaia, aiming at the $10 \mu\text{as}$ range. Given the opto-electrical response variation over the field of view, the mapping between position on the focal plane and angular position on the celestial sphere is a complex relationship, whose non-linearity must be calibrated according to the precision goal. This might be accomplished with purely astronomical methods, i.e. by calibration on the sky, but the rationale for metrology consists in alleviating the related cost, in terms of information, allocated to the stars, thus maximising the scientific return.

Metrology photons should, ideally, follow exactly the optical path of stellar photons; in practice, this is only partially possible, and a mismatch will be present, on entrance pupil, focal plane, and/or the footprint at intermediate optical elements. In Gaia, a complex optical setup is required to inject reference laser beams into the two telescopes without introducing external errors. In a single telescope system, the telescope itself can be used in a sort of auto-collimation scheme,^{5,31} as depicted in Fig. 10: photons are injected close to the focal plane, and the return beam is re-imaged in the conjugated position, after a back-and-forth travel through the optical system thanks to a retro-reflecting mirror. Notably, the back-and-forth travel may compensate or double the disturbances on different degrees of freedom; this will be turned to advantage in the design of a simple demonstration setup, and modified accordingly for a practical implementation on a real telescope, e.g. with multiple beams to disentangle the relevant parameters.

This approach is being tested in OATo lab; the choice of an off-axis parabola to represent the telescope, although more critical with respect to alignment, allows an easier separation of the source/detector from the retro-reflector. The latter region can be exploited for insertion of controlled perturbations to the optical paths, simulating the desired disturbances.

2.3 Multiple Line Of Sight Telescope

The beam combiner concept implemented by Hipparcos was based on two half-mirrors cemented together. This defines a large angle on a plane, i.e. a one-dimensional angle. Simultaneous observation along three, non-planar LOS can similarly be based on three, non-redundant angles, providing an operational definition of a bidimensional angular measurement on the celestial sphere.

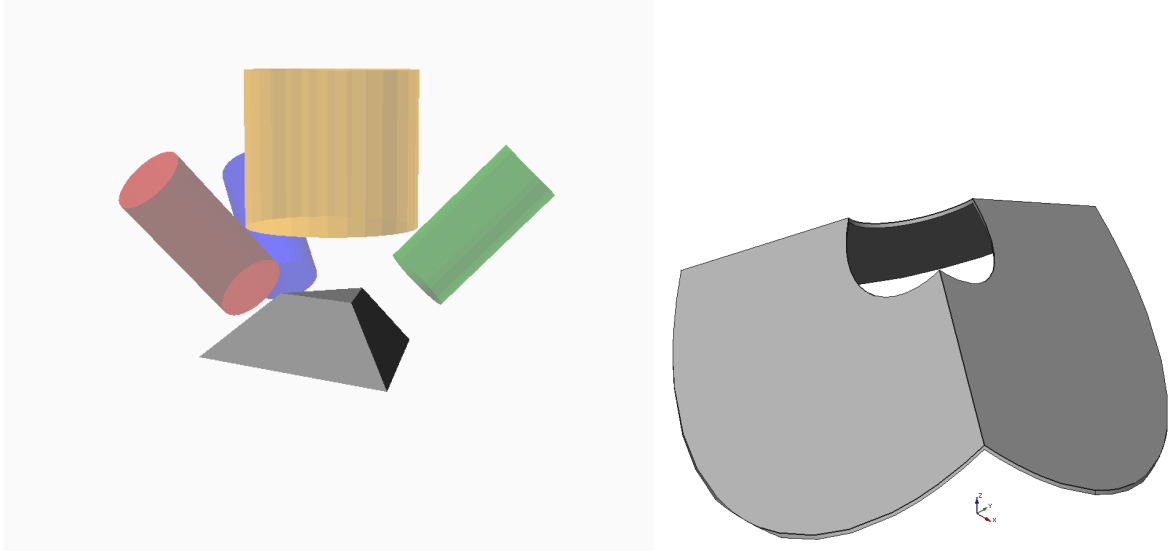


Figure 11. Pyramidal beam combiner principle (left), and a possible lightweight implementation by means of a three mirror assembly.

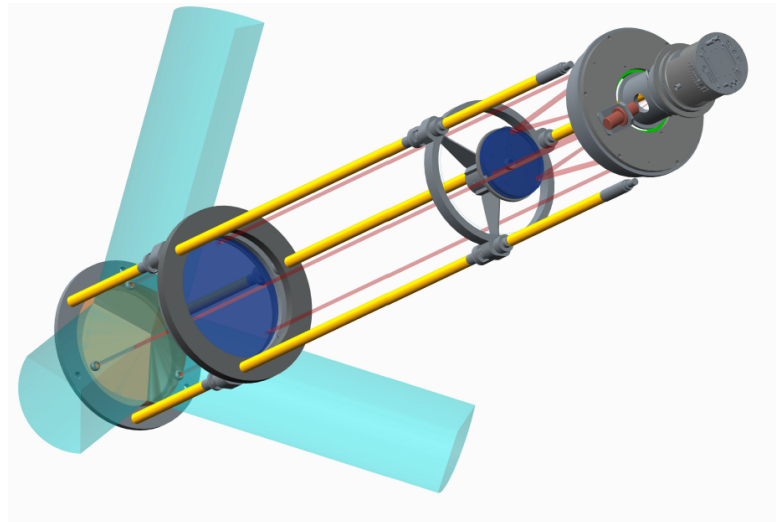


Figure 12. The ASTRA telescope, including the pyramid beam combiner and auto-collimation metrology.

The pyramid approach shown in Fig. 11 (left) provides a simple geometry, in which the three lateral faces of the pyramid feed the overall telescope (yellow) entrance beam from the incoming photons independently coming from three directions, shown respectively in red, blue and green. It may be noted that, reversing the optical paths, i.e. shining a light from the focal plane region, collimated by the telescope optics, the pyramid acts as a wavefront-splitting beam splitter, sending three beams of photons toward the corresponding LOS. In figure, the

central area has been left free, removing the pyramid peak, e.g. to allocate the telescope secondary mirror in a centered system.

This solution may be materialised by a robust and well defined sub-system, e.g. the assembly of three planar mirrors shown in Fig. 11 (right), representing a lightweight device, having removed the pyramid bulk.

The beam combiner represents a convenient location to anchor metrology fiducial points (e.g. retro-reflectors) to monitor the relative LOS stability and/or the telescope optical response. A pictorial representation of the ASTRA telescope, a small size implementation of several of the concepts investigated in this study and planned to be implemented for forthcoming system-level tests, is shown in Fig. 12.

3. CONCLUSIONS

The concepts under investigations are considered to be applicable, under appropriate rescaling, to the implementation of future high precision astrometry experiments. Application examples are presented in other contributions to these proceedings (Riva et al., Gai et al.).

Image centering demonstrates the capability of CMOS and CCD detectors to achieve a nominal precision corresponding to a small fraction of a pixel ($< 1/500$ pixel even in the current initial tests), very close to photon limited expectations.

The design and analysis of a metrology system embedded in a multiple LOS telescope is identifying convenient solutions. Our roadmap considers as the next step the specifications for a small scale experiment aimed at in-flight demonstration of multiple LOS, high precision ($< 1 mas$) astrometry, in preparation for a future implementation on a 1 m class telescope devoted to large angle, μas level measurements for astrophysics and fundamental physics.

ACKNOWLEDGMENTS

The INAF activity has been partially funded by a grant from the Italian Ministry of Foreign Affairs and International Cooperation, and by the Italian Space Agency (ASI) under contracts 2014-025-R.1.2015 and 2018-24-HH.0. RAM acknowledges support from CONICYT/FONDECYT Grant Nr. 1190038 and from the Chilean Centro de Excelencia en Astrofísica y Tecnologías Afines (CATA) BASAL PFB/06.

REFERENCES

- [1] Qi, Z., Yu, Y., Smart, R. L., Lattanzi, M. G., Bucciarelli, B., Spagna, A. r., McLean, B. J., Tang, Z., Jones, H. R. A., Morbidelli, R., Nicastro, L., Vecchiato, A., and Teixeira, R., “A Brief Overview of the Absolute Proper motions Outside the Plane catalog (APOP),” in [*Revista Mexicana de Astronomía y Astrofísica Conference Series*], *Revista Mexicana de Astronomía y Astrofísica Conference Series* **46**, 81 (Oct. 2015).
- [2] Gai, M., Vecchiato, A., Ligori, S., Sozzetti, A., and Lattanzi, M. G., “Gravitation Astrometric Measurement Experiment,” *Exp. Astron.* (2012).
- [3] Gai, M., Vecchiato, A., Ligori, S., Riva, A., Loreggia, D., Lattanzi, M., Busonero, D., and Fienga, A., “Gravitation Astrometric Measurement Experiment (GAME),” in [*Society of Photo-Optical Instrumentation Engineers (SPIE) Conference Series*], *SPIE Conference Series* **8445** (2012).
- [4] Gai, M., Vecchiato, A., Riva, A., Lattanzi, M. G., Sozzetti, A., Crosta, M. T., and Busonero, D., “Astrometric tests of general relativity in the solar system,” *Journal of Physics: Conference Series* **490**, 012240 (mar 2014).
- [5] Gai, M. and et al., “Metrology for AGP - Astrometric Gravitation Probe,” in [*Metrology for Aerospace (MetroAeroSpace)*], 329–334 (Aug. 2015).
- [6] Gaia Collaboration, Prusti, T., de Bruijne, J. H. J., Brown, A. G. A., Vallenari, A., Babusiaux, C., Bailer-Jones, C. A. L., Bastian, U., Biermann, M., Evans, D. W., and et al., “The Gaia mission,” *Astron. Astrophys.* **595**, A1 (Nov. 2016).
- [7] Gaia Collaboration, Brown, A. G. A., Vallenari, A., Prusti, T., et al., “Gaia Data Release 2. Summary of the contents and survey properties,” *Astron. Astrophys.* **616**, A1 (Aug. 2018).
- [8] Lindegren, L., Hernández, J., Bombrun, A., et al., “Gaia Data Release 2. The astrometric solution,” *Astron. Astrophys.* **616**, A2 (Aug. 2018).

- [9] Lattanzi, M. G., “Astrometric cosmology .,” *Mem. Soc. Astr. It.* **83**, 1033 (2012).
- [10] Crosta, M., “Astrometry in the 21st century. From Hipparchus to Einstein,” *Nuovo Cimento Rivista Serie* **42**, 443–510 (Oct. 2019).
- [11] Riva, A., Gai, M., Vecchiato, A., Busonero, D., Lattanzi, M. G., Landini, F., Qi, Z., and Tang, Z., “RAFTER: Ring Astrometric Field Telescope for Exo-planets and Relativity,” *Proc. SPIE*, 114430P (Dec. 2020).
- [12] Perryman, M. A. C., Lindegren, L., Kovalevsky, J., et al., “The HIPPARCOS Catalogue,” *Astron. Astrophys.* **323**, L49–L52 (July 1997).
- [13] Fortenbach, C. D. and Dressing, C. D., “A Framework For Optimizing Exoplanet Target Selection For The James Webb Space Telescope,” *Publ. Astron. Soc. Pac.* **132**, 054501 (May 2020).
- [14] Malbet, F., Léger, A., Shao, M., Goullioud, R., et al., “High precision astrometry mission for the detection and characterization of nearby habitable planetary systems with the Nearby Earth Astrometric Telescope (NEAT),” *Experimental Astronomy* **34**, 385–413 (Oct. 2012).
- [15] Malbet, F., Léger, A., Anglada Escudé, G., Sozzetti, A., et al., “Microarcsecond astrometric observatory Theia: from dark matter to compact objects and nearby earths,” in [*Proc. SPIE*], *Society of Photo-Optical Instrumentation Engineers (SPIE) Conference Series* **9904**, 99042F (July 2016).
- [16] Vallenari, A., “The future of astrometry in space,” *Frontiers in Astronomy and Space Sciences* **5**, 11 (2018).
- [17] Hahn, I., Shao, M., and Turyshev, S. G., “Microarcsecond Astrometry Telescope on the DSG,” in [*Deep Space Gateway Concept Science Workshop*], **2063**, 3015 (Feb. 2018).
- [18] Gai, M., Vecchiato, A., Riva, A., and et al., “Progress on the Astrometric Gravitation Probe design,” *Proc. SPIE* **11443**, 114430N (Dec. 2020).
- [19] Shao, M., Turyshev, S. G., Zhai, C., et al., “Finding Exo-Earths with Precision Space Astrometry,” *Bull. American Astron. Soc.* **51**, 74 (May 2019).
- [20] Malbet, F., Boehm, C., Krone-Martins, A., and et al., “Faint objects in motion: the new frontier of high precision astrometry [submitted],” *Exp. Astron.* (2020).
- [21] Gai, M., Riva, A., Busonero, D., Buzzzi, R., and Russo, F., “Application of Algorithms for High Precision Metrology,” *Publications of the Astronomical Society of the Pacific* **125**, 1383–1392 (Nov. 2013).
- [22] Riva, A., Gai, M., Lattanzi, M. G., et al., “BAM: A metrology device for a high precision astrometric mission,” in [*Rev. Mexicana de Astronomia y Astrofisica Conference Series*], **45**, 35 (Dec. 2014).
- [23] Gai, M., Carollo, D., Delbò, M., Lattanzi, M. G., Massone, G., Bertinetto, F., Mana, G., and Cesare, S., “Location accuracy limitations for CCD cameras,” *Astron. Astrophys.* **367**, 362–370 (Feb. 2001).
- [24] Mendez, R. A., Silva, J. F., and Lobos, R., “Analysis and Interpretation of the Cramér-Rao Lower-Bound in Astrometry: One-Dimensional Case,” *Publ. Astron. Soc. Pac.* **125**, 580–594 (May 2013).
- [25] Gai, M., Busonero, D., and Cancelliere, R., “Performance of an Algorithm for Estimation of Flux, Background, and Location on One-dimensional Signals,” *Publ. Astron. Soc. Pac.* **129**, 054502 (May 2017).
- [26] Echeverria, A., Silva, J. F., Mendez, R. A., and Orchard, M., “Analysis of the Bayesian Cramér-Rao lower bound in astrometry. Studying the impact of prior information in the location of an object,” *aap* **594**, A111 (Oct. 2016).
- [27] Espinosa, S., Silva, J. F., Mendez, R. A., Lobos, R., and Orchard, M., “Optimality of the maximum likelihood estimator in astrometry,” *aap* **616**, A95 (Aug. 2018).
- [28] Lindegren, L., “Photoelectric astrometry - A comparison of methods for precise image location,” in [*IAU Colloq. 48: Modern Astrometry*], Prochazka, F. V. and Tucker, R. H., eds., 197–217 (1978).
- [29] Gai, M., Casertano, S., Carollo, D., and Lattanzi, M. G., “Location Estimators for Interferometric Fringes,” *Publ. Astron. Soc. Pac.* **110**, 848–862 (July 1998).
- [30] Gai, M., Carollo, D., Delbò, M., Lattanzi, M. G., Massone, G., Bertinetto, F., Mana, G., and Cesare, S., “Location accuracy limitations for CCD cameras,” *Astron. Astrophys.* **367**, 362–370 (Feb. 2001).
- [31] Gai, M., Busonero, D., and Riva, A., “A metrology concept for multiple telescope astrometry,” *Proc. SPIE* **8442**, 84421O (Sept. 2012).